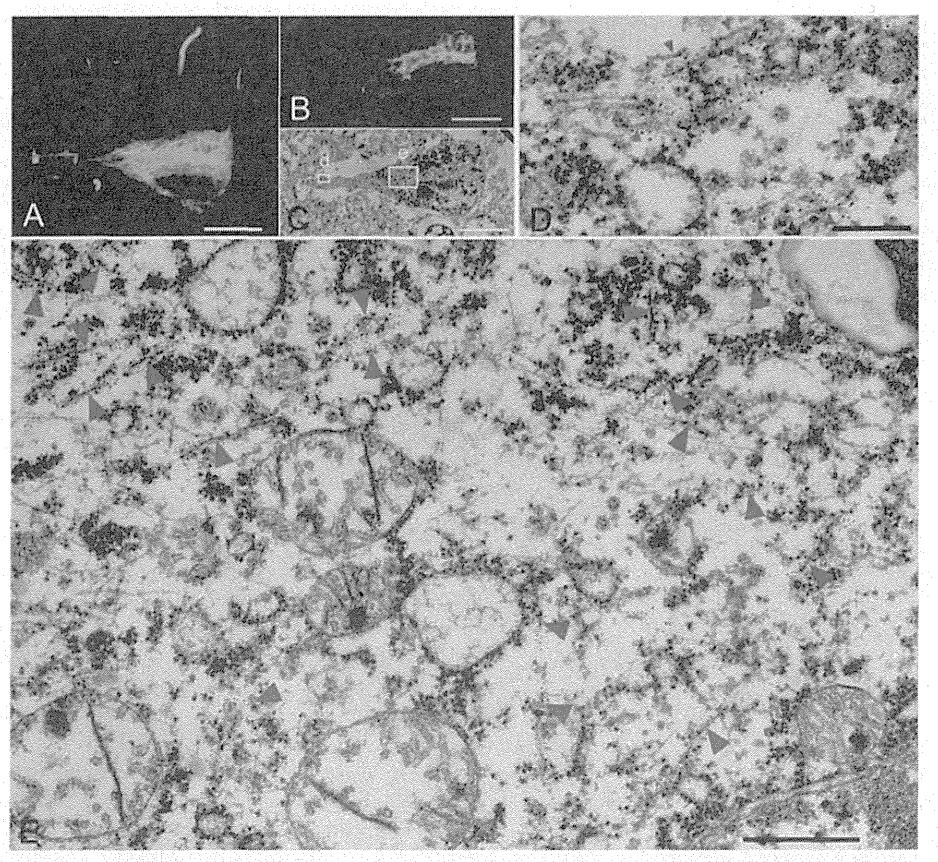

Figure 4 Correlation of immunolabeled LM and EM images of CBD-pretangles. Reticular tau immunoreactivity in the cytoplasm in a pretangle neuron of CBD (case 3) labeled with anti-tau antibody (AT8) visualized with QD 655, also labeled with Alexa 488 for more precise confocal images **(A)**. When compared between LM **(B)** and its exact EM counterpart, reticular tau immunoreactivity in the cytoplasm (**C**, rectangle e) was composed of randomly distributed straight filaments (**E**, arrowheads). Tau immunoreactivity in the dendrite (**C**, rectangle d) on LM corresponded to a few 15-nm straight filaments assembled roughly in parallel. Their arrangement was less tight than that in NFTs in AD. Scale bars in **A-C** = 10 μm; **D** = 250 nm; **E** = 500 nm.

Discussion

The name 'pretangle' was originally used to describe the premature stage of NFT formation in AD [2-4]. However, in CBD, similar structures (also called 'pretangles') are more prevalent than NFTs in the cerebral cortex [6]. It has been unclear whether the pretangles of CBD represent a premature stage before NFT formation and whether they are different from AD-pretangles. Because pretangles are defined only by LM findings [2-4], it would be helpful to compare the corresponding pretangle ultrastructures between the two diseases. However, CBD pretangles in the cortex have not previously been described at the EM level [22-28]. To address this issue, we used a method of correlative light and electron microscopy with QD immunolabeling [19]. This procedure allowed us to observe not only the features of filamentous structures of inclusions but also their intracellular distribution and relationship with cellular organellae.

Using correlated LM and EM images, we observed a distinctive EM feature of AD-pretangles: specifically, a strong tendency to form bundles as a precursor to NFTs. Even in the earliest stages of tau accumulation, small pieces of NFTs could already been seen on the background of diffuse and granular tau staining on LM (Figure 3A) [3,29]. Correlation of the LM and EM images revealed that the granular cytoplasmic staining on LM represented straight filaments (sparsely distributed in the neuronal cytoplasm), and the small tangles represented small bundles of parallel filaments (Figure 3D). Very similar EM findings were reported by Bancher [2], although it remains unclear whether their EM findings really represented LM-defined pretangles or not. Because our method of 3D-oriented immunoEM not only identify pretangles on LM, it is quite sure that our immuno EM findings represent LM-identified pretangles. Moreover, it is further possible to correlates the EM plane (Figure 3C) and its exact counterpart of the corresponding LM plane (Figure 3B), even a small aggregates (Figure 3B arrow) not identifiable on 3D stack image (Figure 3A) can be examined with EM (Figure 3C) for comparison with LM at the extreme

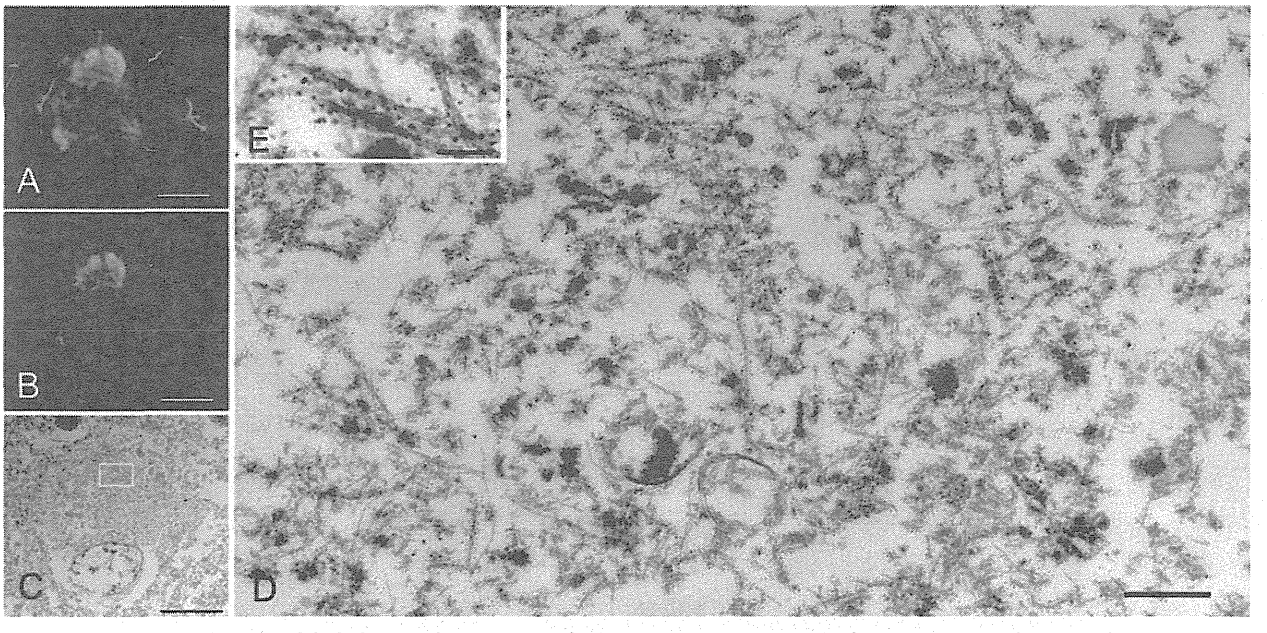

Figure 5 Correlation of immunolabeled LM and EM images of pretangles in a severe case of CBD. In a pretangle neuron from a severe case of CBD (case 4), reticular tau immunoreactivity was denser on 3D reconstruction **(A)**. When focusing on the denser area of round inclusion **(B, C)**, the corresponding EM section contained abundant tau-positive straight filaments that did not form a parallel arrangement **(D)**. These straight filaments were thicker with a diameter of 15–20 nm **(E)**. Scale bars in **A-C** = 10 μm; **D** = 500 nm; **E** = 100 nm.

accuracy. Another feature of AD-pretangles was perinuclear accumulation of tau. Correlation with its EM counterpart showed that a small number of tau-positive 15-nm straight filaments were present around the nuclear membranes of AD-pretangles (Figure 3G-J). It has been reported that PHF or tau-like immunoreactivity may be present in close proximity to the nuclear membrane of mature NFTs in AD [29-32], and this report is the first demonstration of tau-immunolabeled filaments around the nuclear membrane of AD-pretangles. Although intranuclear processes such as aberrant cell cycling may be related to the pathogenesis of AD [33,34], it is unclear how these processes are related to the perinuclear or cytoplasmic deposition of tau.

A similar approach to CBD-pretangles of the cerebral cortex revealed several findings that differed from the features of AD-pretangles and NFTs: (i) random and diffuse distribution of 14–20 nm straight filaments and (ii) paucity of PHFs and fibrillary bundle formation. These ultrastructural architectures may explain the reticular or diffuse tau immmunoreactivity of CBD-pretangles seen on LM (Figures 4 and 5). In dendrites, a small number of straight filaments were observed lying parallel to the dendritic shaft (Figure 4D), similar to the previous reports of dendritic lesions in CBD [8,22]. Even in CBD-pretangles with abundant tau filaments, this random and diffuse distribution of straight filaments was maintained with little NFT formation (Figure 5D). Indeed, this architecture was maintained even in Pick-like inclusions, where tau filaments were randomly assembled and were composed mainly of straight filaments and, to a lesser extent, PHFs with a periodicity of 130–180 nm (Figure 6D-E). Thus, so-called CBD-pretangles are a random accumulation of tau-positive straight filaments, rarely evolving into so-called NFTs even when the filament density is increased. These findings, especially regarding the filamentous structures themselves, were similar to previous findings in CBD (15–20 nm straight filaments or PHFs with a periodicity of 120–180 nm), which were observed in Pick-like inclusions [22-24,27], ballooned neurons [24,28], neuronal inclusions in the brainstem [22,26,28], or an *in vivo* study using CBD brains [25]. However, this study is the first to clarify the EM structures of cortical pretangles in CBD by accurately correlating them with LM images. Authentic Pick bodies in Pick body disease were more solid than pretangles on LM, where abundant tau-positive fibrils, 15 nm in diameter, were randomly arranged without forming PHF [19].

In this study, we greatly enhanced the reliability of pre-embedding immunoEM using QDs. Although QDs are considered suitable for CLEM, their reliability as a reporter for ultrastructural immunolabeling has been debated. The penetration of QD labeling is reported to be limited to several micronmeters from the sample surface [15]. However, we were successful in immunolabeling 25-μm-thick free-floating sections by increasing the incubation time with QD-conjugated secondary antibodies to 8 hr at room temperature. This procedure enabled us

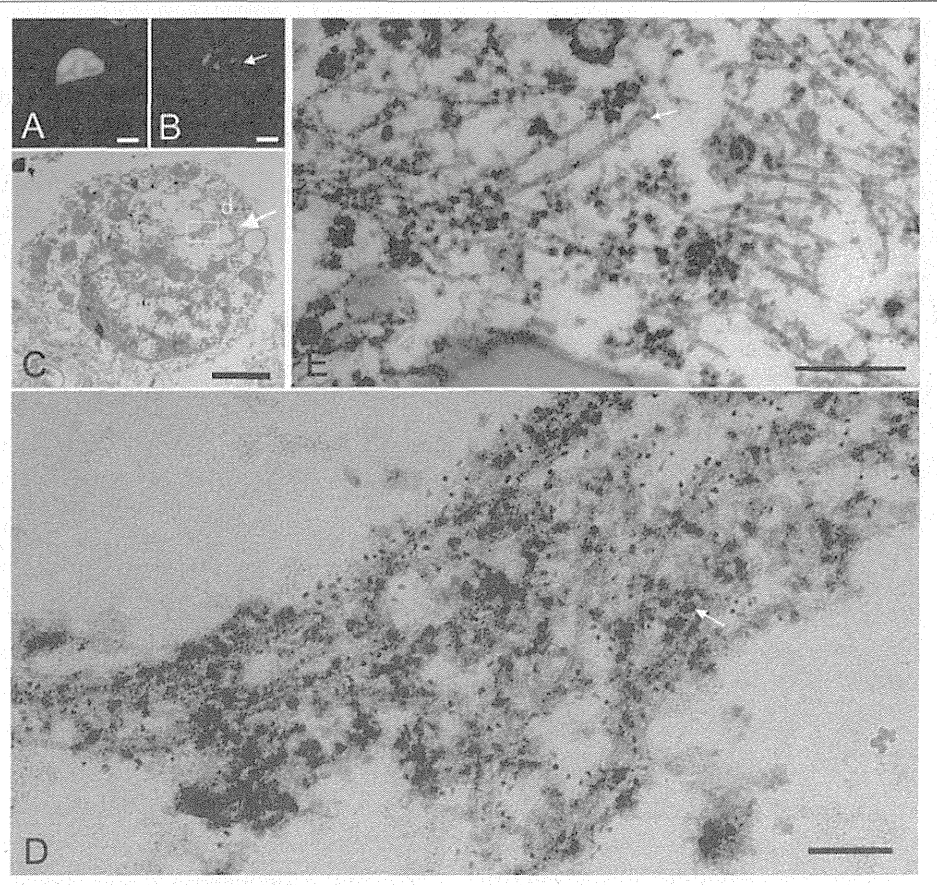

Figure 6 Correlation of immunolabeled LM and EM images of Pick-like inclusions in two CBD cases. A densely packed round inclusion (Pick-like inclusion) from a CBD case (case 3) labeled with anti-PHF antibody (AT8) visualized with QD 655, also labeled with Alexa 488 for more precise confocal images **(A)**. Correlated LM and EM images **(B, C)** showed that tau immunoreactivity around the cavity on LM corresponded to bundles of tau filaments that were not arranged as parallely as in AD (**C**, rectangle d; **D**). Note that these filaments were intermingled with ribosomes (**D**, arrow). **(E)** The ultrastructure of Pick-like inclusions in another case of CBD (case 4) also revealed randomly assembled tau filaments with occasional formation of paired helical filaments (a periodicity of 130 nm, arrow). Scale bars in **A** to **C** = 3 μm; **D** = 50 nm; **E** = 100 nm. **A** to **D**, case 3; **E**, case 4.

Table 2 Similarities and differences between AD-pretangle and CBD-pretangle

		AD		CBD	
		Pretanle	**NFT**	**Pretangle**	**Pick like inclusion**
LM findings (confocal images)	Morphology	Granular	Fibrillary	Reticular	Round, frequent vacuoles
	Perinuclear accentuation	Occiasional	Occasional	None	None
	Size of neurons involved	Small- to large- sized	Small- to large- sized	Medium- to large-sized	Small-sized
EM findings	Density of tau filaments	Very sparse*1	Very dense*2	Sparse	Dense
	Arrangement of tau filaments	*Irregular/regular (focal NFT formation*3)*	*Regular (NFT formation)*	*Irregular*	*Irregular*
	Diameter of straight filaments	About 15 nm	About 15 nm	14-20 nm	About 15 nm
	PHF (a periodicity)	Occasional (about 80 nm)	Frequent (about 80 nm)	None	Occasional (130–180 nm)

IHC, immunohistochemistry; LM, light microscopy; EM, electron microscopy; PHF, paired helical filaments; *1, Density of straight tau filament is more sparse in AD-pretangles than in CBD-pretangles; *2, Density of tau filaments is more dense in AD-NFT than in Pick-like inclusions of CBD; *3, NFT, neurofibrillary tangle signifying a regularly and tightly arranged bundle of straight or paired helical filaments.

to label the entire thickness of floating sections with QDs so that each tau filament was sufficiently labeled (Figures 3 and 4). Consequently, confocal images and immunoEM images could be tightly correlated.

Other disadvantages of QDs are that they have a lower electron density and less distinct contours than colloidal gold for immunolabeling. We previously used EDX spot analysis with STEM to demonstrate the presence of Se and Cd on a pixel basis [19]. This EDX spot analysis, now extended to map the entire EM field, resulted in clear visualization of the position and form of each QD particle. When the corresponding EM image was overlaid, QDs could be readily differentiated from the grayscale cellular backgrounds (e.g., ribosomes) (Figure 2). Similar elemental mapping of Cd has been reported using electron energy loss spectrography (EELS) to detect QDs in ultrathin EM samples [35]. However, compared with EELS, EDX is more suitable for the detection of heavy metals, such as Cd or Se [19,36]. Moreover, because EELS is performed without electron staining, it is difficult to gain sufficient contrast in EM images [35]. Therefore, combined with pre-embedding Q-dot immunoEM and EDX mapping, the use of QDs is one of the most sensitive and distinct ultrastructural immunolabeling techniques available and might be particularly suitable for the correlation of LM/EM images.

Conclusions

Accurate identification of pretangles on LM, followed by EM examination of their exact counterpart was achieved through tau immunolabeling with QD, fluorescent nanocrystals, which are detectable with LM (fluorescence signal) and with EM (electron dense particles with halo). EDX spot analysis to confirm the identity of QD on EM section by showing energy peaks for Cd and Se is now extended to map the entire EM field to highlight QD particles. This improved method with EDX mapping clearly demonstrated for the first time that AD-pretangles showed a strong tendency to form fibrillary tangles even at an early stage, whereas pretangles or Pick-like inclusions in tissue from patients with CBD did not even at an advanced stage. This novel strategy is useful to clarify how molecules other than tau are organized into ultrastructures in the early stages of disease-specific lesions.

Additional files

Additional file 1: Figure S1. Optimal of dilution of QD-conjugated secondary antibodies for ultrastruc-tural immunolabeling.

Additional file 2: Figure S2. Energry dispersive X-ray (EDX) mapping of Quantum dots (QDs).

Competing interests

The authors declare that they have no competing interests.

Authors' contributions

ST, TU, RT and MY designed the study, analysed the data, and drafted the manuscript. ST, TU, IA, YI, MM, MY collected clinical and pathological data. All authors read and approved the final manuscript.

Acknowledgments

This study was supported by Grants-in-Aid for Scientific Research (JSPS KAKENHI 25430057) from the Ministry of Education, Culture, Sports, Science and Technology; a grant from the Japan Foundation for Neuroscience and Mental Health, the Mitsui Life Social Welfare Foundation, and the Tokyo Metropolitan Institute of Medical Science project 'Mechanism for Early Diagnosis and Prevention of Parkinson's disease; and Grants-in-Aid from the Research Committee of CNS Degenerative Diseases, the Ministry of Health, Labour and Welfare of Japan. We are grateful to Takashi Kanemura (Hitachi High-Technologies Corporation) for excellent operation of EDX spot analysis and mapping. Technical contributions by Mr. Kentaro Endo, Ms. Hiromi Kondo (Histology Center) and Ms. Ayako Nakamura (Laboratory of Structural Neuropathology) at Tokyo Metropolitan Institute of Medical Science are gratefully acknowledged.

Author details

[1]Department of Neuropathology, Institute for Medical Science of Aging, Aichi Medical University, Nagakute, Aichi, Japan. [2]Laboratory of Structural Neuropathology, Tokyo Metropolitan Institute of Medical Science, 2-1-6 Kamikitazawa, Setagaya, Tokyo 156-8506, Japan. [3]Department of Neurology, Kyoto University, Kyoto, Japan. [4]Department of Neurology, Higashi Nagoya National Hospital, Nagoya, Aichi, Japan.

Received: 5 November 2014 Accepted: 5 November 2014
Published online: 11 December 2014

References

1. Ross CA, Poirier MA (2004) Protein aggregation and neurodegenerative disease. Nat Med 10(Suppl):S10–S17, doi:10.1038/nm1066
2. Bancher C, Grundke-Iqbal I, Iqbal K, Fried VA, Smith HT, Wisniewski HM (1991) Abnormal phosphorylation of tau precedes ubiquitination in neurofibrillary pathology of Alzheimer disease. Brain Res 539(1):11–18
3. Braak E, Braak H, Mandelkow EM (1994) A sequence of cytoskeleton changes related to the formation of neurofibrillary tangles and neuropil threads. Acta Neuropathol 87(6):554–567
4. Uchihara T (2014) Pretangles and neurofibrillary changes -Similarities and differences between AD and CBD based on molecular and morphological evolution. Neuropathology 34(6):571–7, doi:10.1111/neup.12108
5. Kidd M (1963) Paired helical filaments in electron microscopy of Alzheimer's disease. Nature 197:192–193
6. Dickson DW, Bergeron C, Chin SS, Duyckaerts C, Horoupian D, Ikeda K, Jellinger K, Lantos PL, Lippa CF, Mirra SS, Tabaton M, Vonsattel JP, Wakabayashi K, Litvan I (2002) Office of Rare Diseases neuropathologic criteria for corticobasal degeneration. J Neuropathol Exp Neurol 61(11):935–946
7. Uchihara T, Mitani K, Mori H, Kondo H, Yamada M, Ikeda K (1994) Abnormal cytoskeletal pathology peculiar to corticobasal degeneration is different from that of Alzheimer's disease or progressive supranuclear palsy. Acta Neuropathol 88(4):379–383
8. Tatsumi S, Mimuro M, Iwasaki Y, Takahashi R, Kakita A, Takahashi H, Yoshida M (2014) Argyrophilic grains are reliable disease-specific features of corticobasal degeneration. J Neuropathol Exp Neurol 73(1):30–38, doi:10.1097/NEN.0000000000000022
9. Watanabe S, Punge A, Hollopeter G, Willig KI, Hobson RJ, Davis MW, Hell SW, Jorgensen EM (2011) Protein localization in electron micrographs using fluorescence nanoscopy. Nat Methods 8(1):80–84, doi:10.1038/nmeth.1537
10. Modla S, Czymmek KJ (2011) Correlative microscopy: a powerful tool for exploring neurological cells and tissues. Micron 42(8):773–792, doi:10.1016/j.micron.2011.07.001
11. Jahn KA, Barton DA, Kobayashi K, Ratinac KR, Overall RL, Braet F (2012) Correlative microscopy: providing new understanding in the biomedical and plant sciences. Micron 43(5):565–582, doi:10.1016/j.micron.2011.12.004
12. Caplan J, Niethammer M, Taylor RM 2nd, Czymmek KJ (2011) The power of correlative microscopy: multi-modal, multi-scale, multi-dimensional. Curr Opin Struct Biol 21(5):686–693, doi:10.1016/j.sbi.2011.06.010

13. Giepmans BN, Deerinck TJ, Smarr BL, Jones YZ, Ellisman MH (2005) Correlated light and electron microscopic imaging of multiple endogenous proteins using Quantum dots. Nat Methods 2(10):743–749, doi:10.1038/nmeth791
14. Karreman MA, Agronskaia AV, van Donselaar EG, Vocking K, Fereidouni F, Humbel BM, Verrips CT, Verkleij AJ, Gerritsen HC (2012) Optimizing immuno-labeling for correlative fluorescence and electron microscopy on a single specimen. J Struct Biol 180(2):382–386, doi:10.1016/j.jsb.2012.09.002
15. Deerinck TJ (2008) The application of fluorescent quantum dots to confocal, multiphoton, and electron microscopic imaging. Toxicol Pathol 36(1):112–116, doi:10.1177/0192623307310950
16. Cortese K, Diaspro A, Tacchetti C (2009) Advanced correlative light/electron microscopy: current methods and new developments using Tokuyasu cryosections. J Histochem Cytochem 57(12):1103–1112, doi:10.1369/jhc.2009.954214
17. Faas FG, Barcena M, Agronskaia AV, Gerritsen HC, Moscicka KB, Diebolder CA, van Driel LF, Limpens RW, Bos E, Ravelli RB, Koning RI, Koster AJ (2013) Localization of fluorescently labeled structures in frozen-hydrated samples using integrated light electron microscopy. J Struct Biol 181(3):283–290, doi:10.1016/j.jsb.2012.12.004
18. Heines MA, Guyot-Sionnest P (1996) Synthesis and characterization of strongly luminsecing ZnS-capped CdSe nanocrystals. J Phys Chem 100:468–471
19. Uematsu M, Adachi E, Nakamura A, Tsuchiya K, Uchihara T (2012) Atomic identification of fluorescent Q-dots on tau-positive fibrils in 3D-reconstructed pick bodies. Am J Pathol 180(4):1394–1397, doi:10.1016/j.ajpath.2011.12.029
20. Kanazawa T, Adachi E, Orimo S, Nakamura A, Mizusawa H, Uchihara T (2012) Pale neurites, premature alpha-synuclein aggregates with centripetal extension from axon collaterals. Brain Pathol 22(1):67–78, doi:10.1111/j.1750-3639.2011.00509.x
21. Montine TJ, Phelps CH, Beach TG, Bigio EH, Cairns NJ, Dickson DW, Duyckaerts C, Frosch MP, Masliah E, Mirra SS, Nelson PT, Schneider JA, Thal DR, Trojanowski JQ, Vinters HV, Hyman BT (2012) National Institute on Aging-Alzheimer's Association guidelines for the neuropathologic assessment of Alzheimer's disease: a practical approach. Acta Neuropathol 123(1):1–11, doi:10.1007/s00401-011-0910-3
22. Takahashi T, Amano N, Hanihara T, Nagatomo H, Yagishita S, Itoh Y, Yamaoka K, Toda H, Tanabe T (1996) Corticobasal degeneration: widespread argentophilic threads and glia in addition to neurofibrillary tangles. Similarities of cytoskeletal abnormalities in corticobasal degeneration and progressive supranuclear palsy. J Neurol Sci 138(1–2):66–77
23. Arima K, Uesugi H, Fujita I, Sakurai Y, Oyanagi S, Andoh S, Izumiyama Y, Inose T (1994) Corticonigral degeneration with neuronal achromasia presenting with primary progressive aphasia: ultrastructural and immunocytochemical studies. J Neurol Sci 127(2):186–197
24. Feany MB, Dickson DW (1995) Widespread cytoskeletal pathology characterizes corticobasal degeneration. Am J Pathol 146(6):1388–1396
25. Ksiezak-Reding H, Morgan K, Mattiace LA, Davies P, Liu WK, Yen SH, Weidenheim K, Dickson DW (1994) Ultrastructure and biochemical composition of paired helical filaments in corticobasal degeneration. Am J Pathol 145(6):1496–1508
26. Mori H, Nishimura M, Namba Y, Oda M (1994) Corticobasal degeneration: a disease with widespread appearance of abnormal tau and neurofibrillary tangles, and its relation to progressive supranuclear palsy. Acta Neuropathol 88(2):113–121
27. Lippa CF, Smith TW, Fontneau N (1990) Corticonigral degeneration with neuronal achromasia. A clinicopathologic study of two cases. J Neurol Sci 98(2–3):301–310
28. Wakabayashi K, Oyanagi K, Makifuchi T, Ikuta F, Homma A, Homma Y, Horikawa Y, Tokiguchi S (1994) Corticobasal degeneration: etiopathological significance of the cytoskeletal alterations. Acta Neuropathol 87(6):545–553
29. Kato S, Nakamura H, Otomo E (1989) Reappraisal of neurofibrillary tangles. Immunohistochemical, ultrastructural, and immunoelectron microscopical studies. Acta Neuropathol 77(3):258–266
30. Lowe J, Mirra SS, Hyman B, Dickson DW (2008) Histopathology of Alzheimer's disease. In: Love S, Louis DN, Ellison DW (eds) Greenfield's neuropathology, vol 1, 8th edn. Edward Arnold, London, pp 1031–1152
31. Metuzals J, Robitaille Y, Houghton S, Gauthier S, Leblanc R (1988) Paired helical filaments and the cytoplasmic-nuclear interface in Alzheimer's disease. J Neurocytol 17(6):827–833
32. Hara M, Hirokawa K, Kamei S, Uchihara T (2013) Isoform transition from four-repeat to three-repeat tau underlies dendrosomatic and regional progression of neurofibrillary pathology. Acta Neuropathol 125(4):565–579, doi:10.1007/s00401-013-1097-6
33. Andorfer C, Acker CM, Kress Y, Hof PR, Duff K, Davies P (2005) Cell-cycle reentry and cell death in transgenic mice expressing nonmutant human tau isoforms. J Neurosci 25(22):5446–5454, doi:10.1523/JNEUROSCI. 4637-04.2005
34. Yang Y, Geldmacher DS, Herrup K (2001) DNA replication precedes neuronal cell death in Alzheimer's disease. J Neurosci 21(8):2661–2668
35. Nisman R, Dellaire G, Ren Y, Li R, Bazett-Jones DP (2004) Application of quantum dots as probes for correlative fluorescence, conventional, and energy-filtered transmission electron microscopy. J Histochem Cytochem 52(1):13–18
36. Leapman RD, Ornberg RL (1988) Quantitative electron energy loss spectroscopy in biology. Ultramicroscopy 24(2–3):251–268

doi:10.1186/s40478-014-0161-3
Cite this article as: Tatsumi *et al.*: Ultrastructural differences in pretangles between Alzheimer disease and corticobasal degeneration revealed by comparative light and electron microscopy. *Acta Neuropathologica Communications* 2014 2:161.

Submit your next manuscript to BioMed Central and take full advantage of:

- Convenient online submission
- Thorough peer review
- No space constraints or color figure charges
- Immediate publication on acceptance
- Inclusion in PubMed, CAS, Scopus and Google Scholar
- Research which is freely available for redistribution

Submit your manuscript at
www.biomedcentral.com/submit

BioMed Central

NEUROPATHOLOGY

Neuropathology 2014; **34**, 555–570 doi:10.1111/neup.12143

Symposium: Definition and Differentials – How to Distinguish Disease-Specific Changes on Microscopy

Astrocytic inclusions in progressive supranuclear palsy and corticobasal degeneration

Mari Yoshida

Institute for Medical Science of Aging, Aichi Medical University, Aichi, Japan

Tufted astrocytes (TAs) in progressive supranuclear palsy (PSP) and astrocytic plaques (APs) in corticobasal degeneration (CBD) have been regarded as the pathological hallmarks of major sporadic 4-repeat tauopathies. To better define the astrocytic inclusions in PSP and CBD and to outline the pathological features of each disease, we reviewed 95 PSP cases and 30 CBD cases that were confirmed at autopsy. TAs exhibit a radial arrangement of thin, long, branching accumulated tau protein from the cytoplasm to the proximal processes of astrocytes. APs show a corona-like arrangement of tau aggregates in the distal portions of astrocytic processes and are composed of fuzzy, short processes. Immunoelectron microscopic examination using quantum dot nanocrystals revealed filamentous tau accumulation of APs located in the immediate vicinity of the synaptic structures, which suggested synaptic dysfunction by APs. The pathological subtypes of PSP and CBD have been proposed to ensure that the clinical phenotypes are in accordance with the pathological distribution and degenerative changes. The pathological features of PSP are divided into 3 representative subtypes: typical PSP type, pallido-nigro-luysian type (PNL type), and CBD-like type. CBD is divided into three pathological subtypes: typical CBD type, basal ganglia- predominant type, and PSP-like type. TAs are found exclusively in PSP, while APs are exclusive to CBD, regardless of the pathological subtypes, although some morphological variations exist, especially with regard to TAs. The overlap of the pathological distribution of PSP and CBD makes their clinical diagnosis complicated, although the presence of TAs and APs differentiate these two diseases. The characteristics of tau accumulation in both neurons and glia suggest a different underlying mechanism with regard to the sites of tau aggregation and fibril formation between PSP and CBD: proximal-dominant aggregation of TAs and formation of filamentous NFTs in PSP in contrast to the distal-dominant aggregation of APs and formation of less filamentous pretangles in CBD.

Key words: astrocytic plaque, corticobasal degeneration, fibril formation, progressive supranuclear palsy, tufted astrocyte.

INTRODUCTION

Progressive supranuclear palsy (PSP)[1] and corticobasal degeneration (CBD)[2] have been regarded as distinct clinicopathological entities with hyperphosphorylated four repeat (4R) tau aggregation in neurons and glia, although the recent recognitions of many clinical similarities have increasingly raised more difficulties in the clinical diagnosis of these two disorders. However, microscopic cellular tau pathology has been used to distinguish PSP from CBD.[3–5] PSP is defined primarily by tau-positive neurofibrillary tangles (NFTs), coiled bodies, threads, and tufted astrocytes, in contrast to the ballooned neurons, pretangles, threads, and astrocytic plaques that are characteristic of CBD (Table 1). Because PSP and CBD frequently present similar pathological distributions (Table 1, Fig. 1), a pathological diagnosis may be difficult without the discrimination of abnormal tau inclusions and particularly of the most characteristic and obvious tau morphology, that of astrocytic inclusions.[6] Therefore, it is important to reevaluate and differentiate between tufted astrocytes (TAs) and astrocytic plaques (APs) and to discuss the pathogenesis of these types of inclusions. To address these issues, we reviewed the morphology and differential distribution of

Correspondence: Yoshida Mari, MD, PhD, Institute for Medical Science of Aging, Aichi Medical University, 1-1 Yazakokarimata, Nagakute, Aichi 480-1195, Japan. Email: myoshida@aichi-med-u.ac.jp

Received 16 April 2014; revised 15 June 2014 and accepted 15 June 2014.

© 2014 Japanese Society of Neuropathology

Table 1 Diagnostic pathological findings in progressive supranuclear palsy (PSP) and corticobasal degeneration (CBD)

	PSP	CBD
Lesion	Distribution	
Neuronal loss & gliosis	Affected cortices (variable)	Affected cortices/subcortical white matter (gliosis)
	Globus pallidus	Globus pallidus (variable)
	Subthalamic nucleus	Subthalamic nucleus (variable)
	Substantia nigra	Substantia nigra
		Striatum (caudate and putamen) (gliosis)
	Brainstem tegmentum	Brainstem tegmentum (variable)
	Dentate nucleus	Dentate nucleus (variable)
	Pons and medulla (variable)	Pons and medulla (variable)
Ballooned or achromatic neurons		Affected cortices
Gallyas/4R-tau positive lesions		
Neuronal inclusions	NFTs > Pretangles	Pretangles >> NFTs
	Substantia nigra, oculomotor complex, locus ceruleus, pons, brainstem nuclei, dentate nucleus, globus pallidus, subthalamic nucleus	Affected cortices, substantia nigra, globus pallidus, subthalamic nucleus
	Striatum, thalamus, basal nucleus of Meynert	Striatum, thalamus, basal nucleus of Meynert
	Affected Cortices (variable)	Brainstem nuclei and dentate nucleus
	Spinal cord	Spinal cord
Threads and coiled bodies	Threads and coiled bodies	Threads >> coiled bodies
	Brainstem, cerebellar white matter, globus pallidus, subthalamic nucleus, striatum, thalamus, gray matter and white matter, spinal cord	Subcortical white matter and gray matter, globus pallidus, subthalamic nucleus, striatum, thalamus, brainstem, spinal cord
Astrocytic inclusions	Tufted astrocytes	Astrocytic plaques
	Affected cortices, striatum, brainstem	Affected cortices, striatum

4R-tau, 4 repeat tau; NFTs, neurofibrillary tangles.

pathologic lesions of 95 neuropathologically confirmed PSP cases and 30 CBD cases that were registered at the Institute for Medical Science of Aging, Aichi Medical University. Our focus was on the pathogenesis of astrocytic inclusions, their disease specificity, and their morphological variations.

PROGRESSIVE SUPRANUCLEAR PALSY (PSP)

PSP is a progressive neurodegenerative disorders, described by Steele, Richardson and Olszewski in 1964.[1] It is the second most common form of parkinsonism after Parkinson's disease. Clinical features include abnormal gait, and postural instability, and recurrent falls, supranuclear ophthalmoparesis, cognitive and behavioral changes, pseudobulbar features and dystonia.

Clinical aspects

As noted previously, pathologically confirmed cases of PSP have exhibited some variation of the clinical and pathological features. Therefore, clinical subtypes were proposed to classify PSP: PSP-Richardson, PSP-parkinsonism (PSP-P),[7,8] PSP-pure akinesia with gait freezing (PSP-PAGF),[9] PSP-primary progressive aphasia,[10,11] and PSP-predominant cerebellar involvement (PSP-C).[12,13] The PSP-Richardson type is the prototypical form of PSP that is defined by early falls, early cognitive dysfunction, abnormalities of gaze and postural instabilities. PSP-P represents asymmetric onset, tremor, early bradykinesia, non-axial dystonia and a response to levodopa. Individuals with PSP-PAGF present with the gradual onset of freezing of gait or speech, absent limb rigidity and tremor, a lack of sustained response to levodopa, and no dementia or ophthalmoplegia in the first 5 years of disease. PSP-primary progressive aphasia is defined by the presence of primary progressive aphasia, or progressive nonfluent aphasia. Individuals with PSP-C develop cerebellar-predominant ataxia as the initial and principal symptom.

Neuropathology

Neuropathological diagnostic criteria

The pathological criteria for the diagnosis of PSP are well established and include specific neuronal loss with gliosis and neurofibrillary tangles (NFTs) in the subcortical and brainstem nuclei and in the cerebellar dentate nucleus with the pathological accumulation of abnormally phosphorylated microtubule-associated protein tau into filamentous deposits.[14] The NINDS diagnostic criteria for PSP and related disorders are pertinent for typical PSP,

© 2014 Japanese Society of Neuropathology

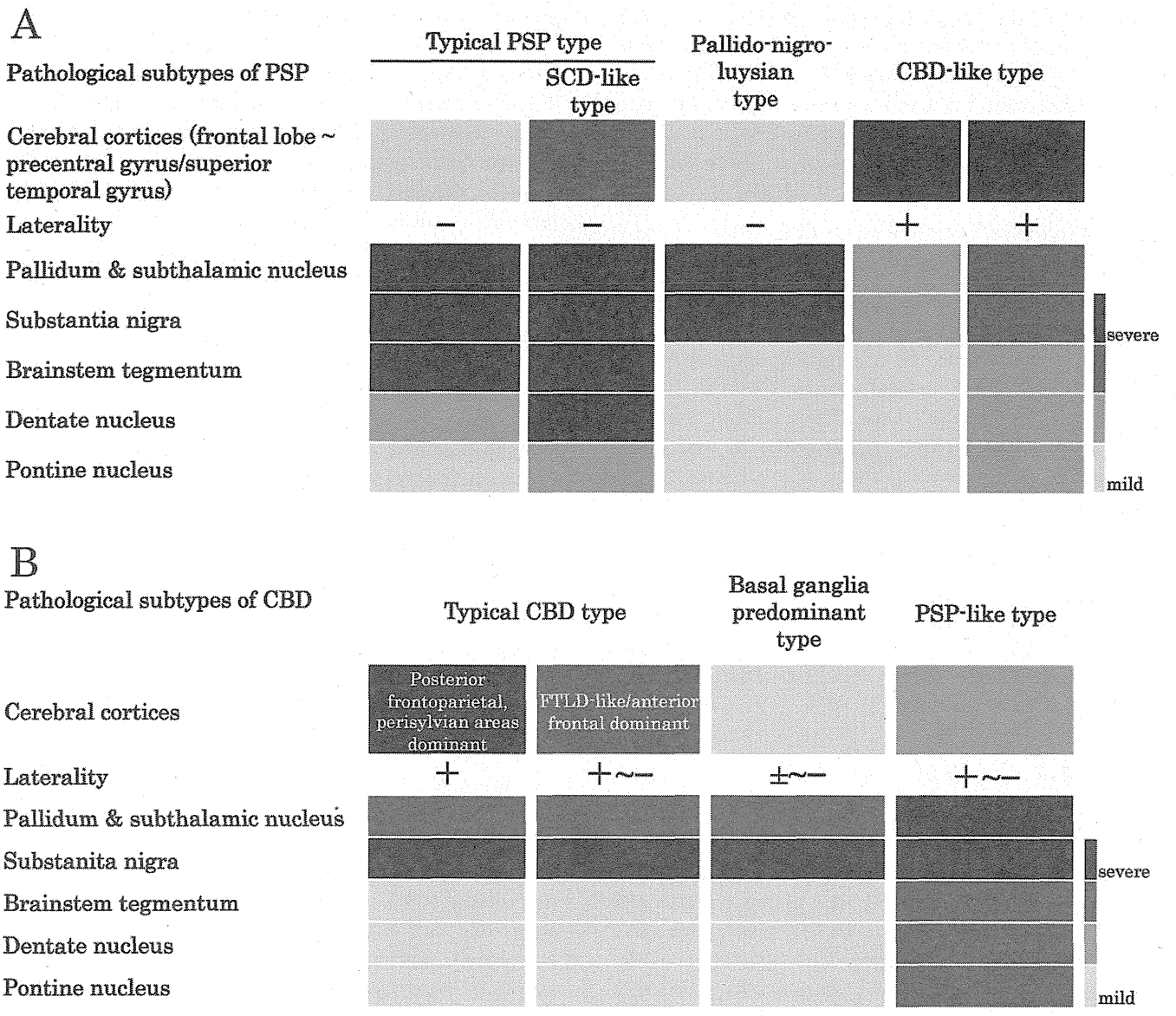

Fig. 1 The group of pathological subtypes in PSP (A) and CBD (B). (A) The pathological subtypes in PSP is generally divided into three representative types: typical PSP type, pallido-nigro-luysian type (PNL type), and CBD-like type, according to the distribution of the lesions and the severity. The spinocerebellar degeneration (SCD)-like type is associated with severe degeneration of the dentate nucleus, superior cerebellar peduncles, cerebellar cortex, white matter and pontine tegmentum and base, which are frequently associated with frontal involvement. The PNL type shows relatively restricted changes in pallido-nigro-luysian lesions. The CBD-like type is accompanied by more severe, asymmetrical cortical changes and a variable degeneration of the basal ganglia, brainstem and cerebellar dentate nucleus. (B) The pathological subtypes of CBD is generally divided into three representative types: typical CBD type, basal ganglia-predominant type, and PSP-like type, according to the distribution of the lesions and the severity. The typical CBD type shows dominant cortical involvement with laterality in the posterior frontoparietal or perisylvian areas. Some cases exhibit anterior frontal-dominant cortical degeneration, such as frontotemporal lobar degeneration. The basal ganglia-predominant type reveals severe involvement of the pallidum and subthalamic nucleus, with relatively mild cortical degeneration without distinct laterality. The PSP-like type shows severe degeneration of the brainstem and dentate nucleus similar to that seen in PSP, in addition to the variable cortical involvement.

which conforms to the original description, and atypical PSP, which consists of histologic variants where the severity or distribution of abnormalities, or both, deviate from the typical pattern; these criteria are also relevant for combined PSP, in which typical PSP is accompanied by concomitant infarcts in the brainstem, basal ganglia, or both.[3,12] Microscopic findings include a high density of NFTs and neuropil threads in at least three of the following areas: the pallidum, subthalamic nucleus, substantia nigra, or pons. In addition, a low to high density of NFTs or neuropil threads is found in at least three of the following areas: the striatum, oculomotor complex, medulla, or dentate nucleus. A clinical history

© 2014 Japanese Society of Neuropathology

that is compatible with PSP is also required for diagnosis according to this set of criteria. These criteria have come to define the typical clinicopathological PSP cases. However, based on these criteria, it was recommended that atypical PSP should be excluded as a PSP subtype because further neuropathological studies of this entity were needed.

Neuropathological reevaluation of PSP cases

Among 95 pathologically confirmed PSP cases, 25 cases were associated with other significant diseases. Two of these cases were associated with Alzheimer's disease, 12 with Parkinson's disease or dementia with Lewy bodies (DLB), 1 with multiple system atrophy, 1 with SCA6 and DLB, 1 with amyotrophic lateral sclerosis, 1 with traumatic brain injury, 4 with cerebrovascular disease, 1 with glioblastoma, and 2 cases were without detailed information. With the exception of these 25 cases, 70 cases were analyzed and had the following characteristics: a mean age at onset of 67 years (range 39–92 years), a mean disease duration of 8 years (range 1–28 years), and a mean age at death of 75 years (range 49–106 years). PSP is a sporadic disease, although approximately 7% of affected individuals have a family history of neurological disorders, including parkinsonism or dementia.

Macroscopic and microscopic findings

The macroscopic examination of the brain in typical PSP reveals mild frontal atrophy including precentral gyrus, particularly in the convexity (Fig. 2A). The brainstem and cerebellum are mildly atrophic. The globus pallidus and subthalamic nucleus usually show a brownish atrophy. The third ventricle may be enlarged. The tegmentum of the midbrain and pons also shows atrophy. The substantia nigra shows discolored, while the locus ceruleus is often relatively preserved. The cerebellar dentate nucleus, and the superior cerebellar peduncle are atrophic.

The microscopic findings indicate neuronal loss and gliosis with NFTs, which appear globose in appearance, in the basal ganglia, thalamus, brainstem, and cerebellum (Table 1, Fig. 3). The thalamus has mild to moderate neuronal loss and gliosis, while the putamen and the caudate show mild gliosis. The most affected nuclei are the globus pallidus, subthalamic nucleus and substantia nigra. The affected regions of the brainstem are as follows: midbrain tegmentum including the superior colliculus, periaqueductal gray matter, oculomotor nuclei, locus ceruleus, pontine tegmentum, pontine nuclei, medullary tegmentum and the inferior olivary nucleus. The dentate nucleus usually exhibits grumose degeneration. The superior cerebellar peduncles are atrophic, and the cerebellar cortex may show mild loss of Purkinje cells with mild atrophy of the white matter. The medullary tegmentum may be atrophic with myelin pallor. The cerebral cortices show mild gliosis especially in the premotor and precentral gyrus in the convexity. The spinal cord, especially the cervical segment, is usually involved, particularly in the medial division of the anterior horn and intermediate gray matter.[15–17] Transverse sections of the spinal cord often show myelin pallor in the anterolateral funiculus in the cervical and thoracic segments. Immunohistochemistry for phosphorylated tau or modified Gallyas silver staining reveals NFTs, pretangles in neurons, tufted astrocytes, coiled bodies in oligodendrocytes, and threads (Table 1, Fig. 3).

Tufted astrocytes

TAs are defined as radial arrangements of thin and long branching fibers without collaterals that course continuously through the cytoplasm to the distal processes of astrocytes (Fig. 3d–j,m,n).[6,18] "Tufts of abnormal fiber," as described in PSP by Hauw *et al.*,[19] is the root of the nomenclature for "tufted astrocytes," although their cellular characterization was not mentioned in their study. Tufted astrocytes were described by Hauw *et al.*[19] as star-like tufts of fibers devoid of degenerative features and without amyloid cores that are clearly distinguishable with Bodian stain as well as with tau immunocytochemistry. The astrocytic nature of the cells that contain the tufted-type inclusions was confirmed by the double-labeling of sections with antibodies to GFAP, CD44 and abnormal tau.[20–22] Cytoplasmic staining is usually not conspicuous within TAs

Fig. 2 Macroscopic findings of typical PSP type (A), pallido-nigro-luysian (PNL)- type (B) and CBD-like type (C).
(A) Macroscopic findings in coronal sections of typical PSP show mild frontal atrophy in the convexity (a), atrophy of the pallidum and subthalamic nucleus (a, arrow), atrophy of the brainstem tegmentum (b), loss of pigment in the substantia nigra (b, arrow) with preservation of pigment in the locus ceruleus, and atrophy of the cerebellar dentate nucleus (c). Bar = 2 cm.
(B) Macroscopic findings in PNL-type PSP reveal severe atrophy of the pallidum and the subthalamic nucleus (a) and depigmentation of the substantia nigra (b), with relative preservation of the brainstem tegmentum (b) and cerebellar dentate nucleus (c). The PNL-type sometimes shows atypical TAs, which demonstrates proximal dominant tau accumulations (d, e). d, Gallyas silver stain; e, AT8 immunohistochemistry; a, b, c, bar = 2 cm; e, bar = 10 μm.
(C) Macroscopic findings in CBD-like type PSP indicate left side-predominant degeneration of the cerebral cortices and the basal ganglia (a–d) with relatively mild atrophy of the brainstem (e). Microscopically typical TAs are observed in the basal ganglia and cerebral cortices (f, g). a, c, Klüver-Barrera stain; b, d, Holzer stain; f, Gallyas silver stain; g, AT8 immunohistochemistry; bar = 10 μm.

© 2014 Japanese Society of Neuropathology

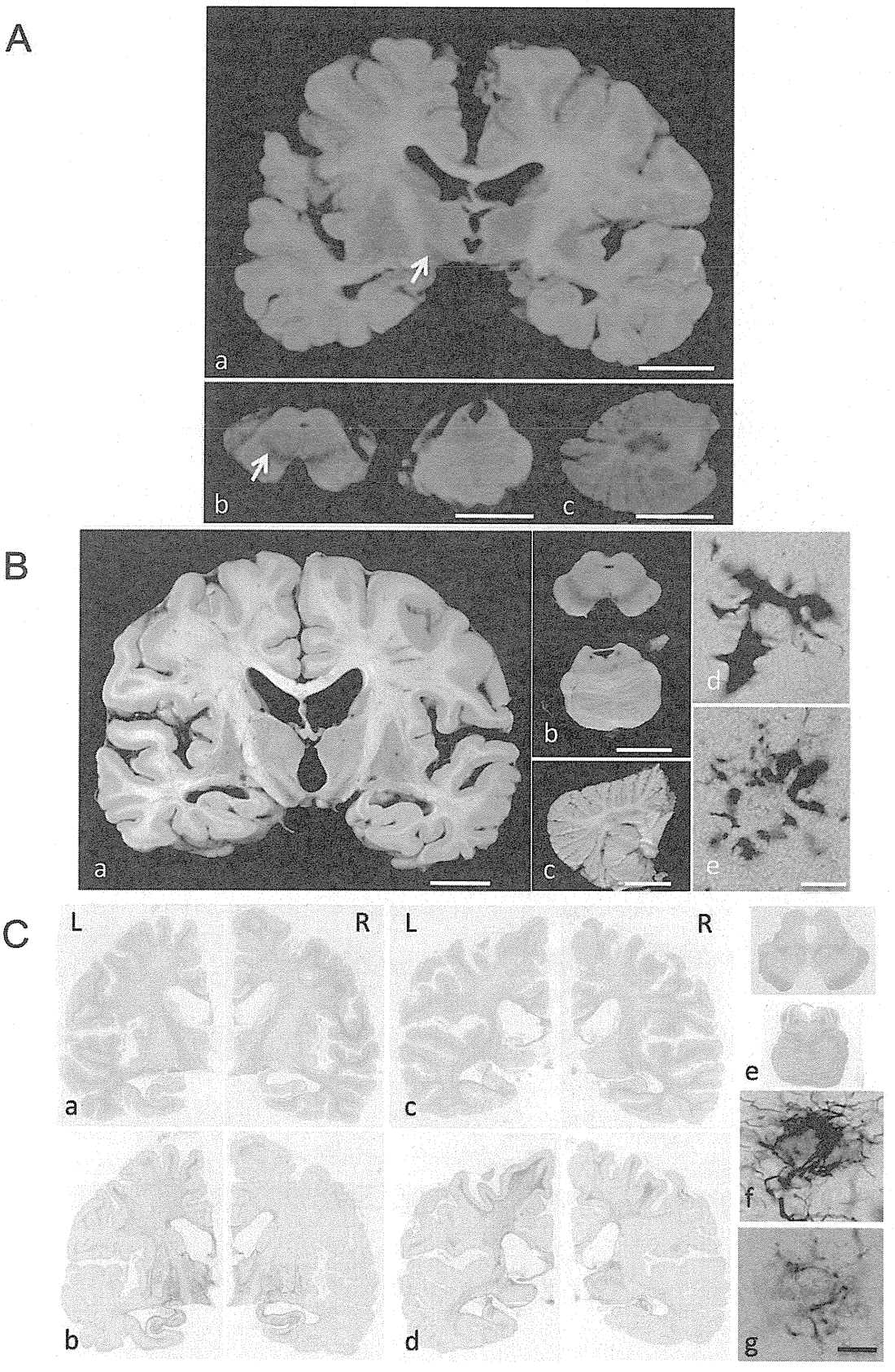

© 2014 Japanese Society of Neuropathology